

# NH<sub>3</sub>(1,1) survey toward southern hemisphere HII regions. I

J.W.S. Vilas-Boas<sup>1</sup> and Z. Abraham<sup>2</sup>

<sup>1</sup> Centro de Radio Astronomia e Aplicações Espaciais (CRAAE-INPE), CRAAM, Inst. Presbiteriano Mackenzie, R. Consolação 89, CEP 01302-000 São Paulo, SP, Brazil

<sup>2</sup> Instituto Astronômico e Geofísico, Universidade de São Paulo, Av. M. Stefano 4200, CEP 04301-904 São Paulo, SP, Brazil

Received 19 July 1999 / Accepted 20 January 2000

**Abstract.** The (J,K)=(1,1) metastable ammonia line was searched for in the direction of more than one hundred southern HII regions located between 270° and 15° in galactic longitude, resulting in new detections toward 21 of them. Ammonia detection rate was about 30 % towards all directions except in the longitude interval 270°–290° where no ammonia lines were found in the 15 selected HII regions. A high detection rate ( $\geq 0.6$ ) was observed toward positions where IRAS point sources with color indices of ultra-compact HII regions were in the beam of the telescope. An anticorrelation between the number of detected NH<sub>3</sub> sources and the distance to the Galactic Center was found, compatible with the observed gradient in N abundance. From the value of this gradient and the detection rate of ammonia lines toward HII regions, it is inferred that the number of ammonia sources must be proportional to the inverse of the column density of the molecular cloud.

**Key words:** ISM: abundances – ISM: clouds – ISM: molecules – radio lines: ISM

## 1. Introduction

Since its discovery (Cheung et al. 1968), ammonia has been observed in the Galaxy via several transitions, particularly the metastable lines (J=K, K). The spectral lines of this molecule are a powerful tool to determine the physical conditions of the clouds and good tracers of dense molecular gas. Surveys of ammonia lines have been made from the northern hemisphere toward dark clouds (e.g. Myers & Benson 1983) and giant and ultra-compact HII regions (McDonald et al. 1981, Churchwell et al. 1990). However, only recently has an extended NH<sub>3</sub> survey been published toward dense condensations of the southern hemisphere dark clouds (Bourke et al. 1995 a, b) and only a few positions have been observed toward HII regions (Jauncey et al. 1981, Scalise et al. 1981, Gardner et al. 1985, Vilas-Boas et al. 1988).

In this paper we present the results of a (J,K)=(1,1) survey toward 108 southern hemisphere HII regions. The selected positions are the peaks of H109  $\alpha$  recombination line emission with temperatures larger than 0.05 K, observed by Wilson et al (1970). They represent roughly 73 % of the HII regions in the

sample, which was compiled from three surveys of continuum sources at 6, 11 and 20 cm in the direction  $355^\circ > l > 280^\circ$  and  $4^\circ > b > -4^\circ$ .

## 2. Instrument and observing technique

The observations were made during June and July 1996 using the 13.7 m radome enclosed radio telescope placed at the Itapetinga Radio Observatory. The radiotelescope resolution at the NH<sub>3</sub>(1,1) transition is 4.2 arc min. The receiver front-end consisted of a cooled HEMPT amplifier giving 50 db total gain. The single side band receiver temperature was typically 90 K and the total system temperature oscillated between 130 and 220 K. A circularly polarized corrugated horn was used in the observations. The aperture and beam efficiency were 0.37 and 0.63 respectively. The back-end was an acousto-optical spectrometer with 70 kHz resolution and total bandwidth of 41 MHz. The central frequency and frequency resolution were frequently checked by injecting monochromatic signals at the intermediate frequency stage. The spectra were taken using the ON-OFF total-power observing technique, switching between positions every 20 s. The signal was calibrated against a 15 K noise source and a room temperature load, to obtain the gain and correct for atmospheric attenuation (Abraham and Kokubun, 1992). Systematic observations of the transitions (J,K)=(1,1), (2,2) and (3,3) toward NGC 6334 and Orion A, which are well known NH<sub>3</sub> sources, were performed in order to check the absolute intensity. The observations were made with the sources above 30° in elevation and special care was taken to guarantee that the OFF position, generally 20' away in azimuth, fell outside the HII region. Also, we did not detect any absorption features, as would be observed if the molecular cloud were included in the OFF position and even small velocity gradients were present in the cloud.

## 3. Data reduction and observational results

We used the Drawspec software to analyse the spectra, a baseline was subtracted and the line parameters determined by fitting Gaussian functions. The observational results obtained toward 108 Galactic HII regions are shown in Table 1. Columns (1) and (2) give the names of the HII regions, Columns (3) and (4)

**Table 1.** The NH<sub>3</sub>, (J=K=1) Observational results toward Southern HII regions

Gal. Coord (l+b)	Name	RA (1950) (h m s)	Dec (1950) (° ' ")	T <sub>A</sub> <sup>*</sup> K	NH <sub>3</sub> (1,1) V km s <sup>-1</sup>	ΔV km s <sup>-1</sup>	V <sub>LSR</sub> (H109α) km s <sup>-1</sup>	d1 kpc	d2 kpc	R kpc	Comments
209.0-19.4*	Ori A	05 32 50	-05 25 36	0.38 [0.04]	-1.0	3.5	-2.8				H <sub>2</sub> CO
267.9-1.1	RCW38	08 57 22	-47 19 04	[0.07]			-3.0				H <sub>2</sub> CO
267.8-0.9	RCW38	08 57 40	-47 07 12	[0.03]			7.8	1.5		8.1	H <sub>2</sub> CO
265.1+1.5	RCW36	08 57 38	-43 33 36	0.17 [0.02]	1.4	2.9	2.8	0.6		8.0	H <sub>2</sub> CO
268.0-1.1		08 58 05	-47 20 12	[0.02]			1.8	0.6		7.9	
268.4-0.8		09 00 15	-47 32 36	0.24 [0.04]	2.1	3.4	3.0	0.1		8.0	H <sub>2</sub> CO, IRAS
274.0-1.1	RCW42	09 22 47	-50 53 00	[0.05]			2.0	1.6		7.9	H <sub>2</sub> CO
281.0-1.5		09 57 26	-56 02 00	[0.04]			0.0	3.0		7.9	H <sub>2</sub> CO
282.0-1.2		10 04 53	-56 57 30	[0.04]			22.0	5.1		8.5	H <sub>2</sub> CO
284.3-0.3	RCW49	10 22 20	-57 32 00	[0.04]			7.0	4.5		8.1	H <sub>2</sub> CO
287.3-0.9		10 39 50	-59 29 11	[0.05]			-17.0				
287.4-0.6	RCW53	10 41 36	-59 19 11	[0.04]			-20.0				H <sub>2</sub> CO
287.5-0.6		10 42 50	-59 22 59	[0.04]			-23.0				
287.6-0.9		10 42 09	-59 42 17	[0.05]			-24.8				
287.7-0.6		10 43 54	-59 29 29	[0.04]			10.5	5.6		8.2	
287.8-0.8		10 43 43	-59 40 29	[0.04]			-20.0				
287.9-0.9		10 44 09	-59 50 17	[0.05]			-19.0				
287.9-0.8		10 44 53	-59 44 41	[0.05]			-25.0				
289.1-0.4		10 54 29	-59 49 48	[0.05]			27.0	6.9	7.4	8.6	H <sub>2</sub> CO
289.8-1.1	RCW54	10 56 51	-60 50 48	[0.05]			21.0	6.7		8.5	
291.3-0.7	RCW57	11 09 45	-61 02 36	0.14 [0.05]	-19		-20.0	2.2	3.5	7.4	H <sub>2</sub> CO, IRAS
291.6-0.4		11 12 54	-60 52 57	[0.05]			14.0	6.7		8.3	H <sub>2</sub> CO
291.6-0.5	RCW57	11 12 53	-60 59 24	[0.05]			10.0	6.5		8.2	H <sub>2</sub> CO
295.1-1.6	RCW62	11 37 47	-63 08 42	[0.03]			-20	1.6	5.1	7.4	
295.2-0.6		11 41 05	-62 09 12	[0.04]			51.0	12.2		11.4	
298.8-0.3		12 12 38	-62 39 12	[0.04]			25.0	8.9	9.4	8.6	H <sub>2</sub> CO
298.9-0.4		12 12 44	-61 44 48	[0.05]			25.0	9.0	9.4	8.6	H <sub>2</sub> CO
301.0+1.2	RCW65	12 32 03	-61 22 54	0.15 [0.04]	-45	3.5	-46.0				H <sub>2</sub> CO, IRAS
301.1+1.0		12 33 11	-61 34 48	0.20 [0.04]	-47	2.0	-48.0				H <sub>2</sub> CO
305.1+0.1		13 07 06	-62 22 36	0.30 [0.04]	-34	2.0	-38.8				H <sub>2</sub> CO
305.2+0.0	RCW74	13 08 03	-62 29 12	[0.03]			-38.0	2.4	6.8	6.8	H <sub>2</sub> CO
305.2+0.2		13 08 23	-62 17 30	0.15 [0.05]	-38		-39.0	2.4	6.7	6.8	H <sub>2</sub> CO, IRAS
305.6+0.0		13 11 06	-62 28 54	[0.05]			-45.0	3.0	6.2	6.6	H <sub>2</sub> CO
308.6+0.6		13 36 37	-61 29 00	[0.05]			-52.0	3.3	6.6	6.4	H <sub>2</sub> CO
308.7+0.6	RCW79	13 37 18	-61 29 48	0.16 [0.03]	-52	2.3	-46.0	2.7	7.1	6.6	H <sub>2</sub> CO
311.5+0.4		14 00 01	-61 02 12	[0.09]			-65.0	4.3	6.1	6.0	H <sub>2</sub> CO
311.6+0.3		14 01 16	-61 05 36	0.13 [0.05]	-58		-63.0	3.5	7.0	6.2	H <sub>2</sub> CO, IRAS
311.9+0.1		14 03 52	-61 13 06	[0.05]			-47.0	2.6	8.0	6.5	H <sub>2</sub> CO
311.9+0.2		14 03 49	-61 05 18	[0.05]			-50.0	2.8	7.8	6.4	H <sub>2</sub> CO
314.2+0.4		14 21 16	-60 09 12	[0.06]			-55.0	3.0	8.0	6.2	
316.8-0.1		14 41 31	-59 36 54	0.20 [0.06]	-39		-36.0	1.8	9.7	6.7	H <sub>2</sub> CO, IRAS
317.0+0.3		14 41 45	-59 13 36	[0.05]			-50.0	2.6	9.0	6.3	
317.3+0.2		14 44 14	-59 08 18	[0.04]			-46.0	2.4	9.2	6.4	
319.2-0.4		14 59 14	-58 51 42	[0.07]			-23.0	1.1	10.8	7.1	H <sub>2</sub> CO
319.4+0.0		14 59 23	-58 24 30	[0.05]			-13.0	0.7	11.4	7.4	H <sub>2</sub> CO
320.2+0.8	RCW87	15 01 34	-57 19 24	0.16 [0.01]	-32	4.2	-35.0	1.8	10.4	6.6	H <sub>2</sub> CO
320.3-0.2		15 06 04	-58 06 12	0.10 [0.05]			-7.0	0.3	11.8	7.6	H <sub>2</sub> CO
321.0-0.5	RCW91	15 12 06	-58 00 30	[0.05]			-60.0	3.1	9.1	5.8	H <sub>2</sub> CO
321.1-0.5	RCW91	15 12 45	-57 59 36	[0.05]			-60.0	3.1	9.2	5.8	H <sub>2</sub> CO
322.2+0.6	RCW92	15 14 49	-56 27 54	0.14 [0.06]			-51.0	2.6	9.9	6.1	H <sub>2</sub> CO
326.5+0.9		15 38 33	-53 48 54	0.31 [0.02]	-39	3.6	-40.0	2.1	11.1	6.3	H <sub>2</sub> CO
326.7+0.6*		15 40 56	-53 57 12	0.76 [0.05]	-47	3.6	-50.0	2.6	10.6	5.9	H <sub>2</sub> CO, IRAS
327.3-0.5*	RCW97	15 49 12	-54 26 30	0.28 [0.02]	-53	5.5	-40.0	2.1	11.2	6.2	H <sub>2</sub> CO
328.0-0.1		15 50 54	-53 39 24	[0.04]			-40.0	2.1	11.3	6.2	
328.3+0.4		15 50 15	-53 02 46	0.16 [0.04]	-98		-95.0	5.2	8.2	4.4	H <sub>2</sub> CO, IRAS
330.9-0.4		16 06 27	-51 58 36	[0.05]			-50.0	2.7	11.0	5.7	H <sub>2</sub> CO
331.0-0.2		16 06 20	-51 42 30	[0.04]			-90.0	4.9	8.8	4.3	H <sub>2</sub> CO
331.1-0.2		16 07 11	-51 42 53	[0.04]			-81.0	4.4	9.5	4.6	
331.4+0.0		16 07 18	-51 23 06	0.14 [0.04]	-68		-80.0	4.3	9.6	4.6	H <sub>2</sub> CO
331.1-0.5		16 08 23	-51 55 30	[0.03]			-68.0	3.7	10.2	5.0	H <sub>2</sub> CO
331.3-0.2		16 07 36	-51 34 54	0.16 [0.04]	-85	3.3	-84.0	-4.5	9.3	4.5	H <sub>2</sub> CO
331.3-0.3		16 08 33	-51 39 24	[0.04]			-60.0	3.2	10.6	5.3	H <sub>2</sub> CO
331.5-0.1		16 08 21	-51 21 11	0.36 [0.03]	-91	4.7	-95.0	5.2	8.7	4.2	H <sub>2</sub> CO
332.2-0.5		16 12 52	-51 10 06	[0.05]			-55.0	3.0	10.9	5.4	H <sub>2</sub> CO
332.5-0.1		16 13 17	-50 40 18	[0.03]			-56.0	3.1	10.9	5.3	H <sub>2</sub> CO
332.7-0.6	RCW106	16 15 58	-50 56 00	complex			-47.0	2.6	11.4	5.7	H <sub>2</sub> CO
332.8-0.6	RCW106	16 16 25	-50 47 18	0.17 [0.05]	-59	5.0	-57.0	3.2	10.9	5.3	H <sub>2</sub> CO, IRAS
333.0-0.4		16 16 51	-50 33 12	0.23 [0.03]	-59	5.0	-53.0	3.0	11.1	5.4	H <sub>2</sub> CO
333.1-0.4*		16 17 13	-50 28 18	0.33 [0.05]	-54	2.9	-50.0	2.8	11.3	5.5	H <sub>2</sub> CO, IRAS
333.2-0.1		16 15 56	-50 12 18	0.21 [0.04]	-92	3.4	-90.0	4.9	9.2	4.1	H <sub>2</sub> CO
333.3-0.4*		16 17 45	-50 19 18	0.34 [0.03]	-48	4.7	-50.0	2.8	11.3	5.5	H <sub>2</sub> CO, IRAS
333.6-0.1		16 17 53	-49 53 54	0.22 [0.04]	-19	2.5	-50.0	2.8	11.3	5.5	H <sub>2</sub> CO
333.6-0.2		16 18 26	-49 58 54	0.20 [0.07]	-73		-50.0	2.8	11.3	5.5	H <sub>2</sub> CO
333.7-0.5		16 19 58	-50 06 12	[0.05]			-50.0	2.9	11.3	5.5	

**Table 1.** (continued)

Gal. Coord (l+b)	Name	RA (1950) (h m s)	Dec (1950) (° ' ")	T <sub>A</sub> <sup>*</sup> K	NH <sub>3</sub> (1,1) V km s <sup>-1</sup>	ΔV km s <sup>-1</sup>	V <sub>LSR</sub> (H109α) km s <sup>-1</sup>	d1 kpc	d2 kpc	R kpc	Comments
335.8-0.2		16 27 27	-48 24 06	[0.08]			-52.0	3.1	11.3	5.2	H <sub>2</sub> CO
336.4-0.2		16 29 52	-47 56 54	[0.06]			-68.0	4.0	10.5	4.6	H <sub>2</sub> CO
336.4-0.3		16 30 33	-47 59 06	0.15 [0.05]	-92		-90.0	5.1	9.4	3.8	H <sub>2</sub> CO
337.3-0.1		16 33 27	-47 16 24	0.25 [0.07]	-39		-53.0	3.2	11.3	5.1	H <sub>2</sub> CO
337.6+0.0		16 34 30	-46 58 06	[0.05]			-55.0	3.4	11.2	5.0	H <sub>2</sub> CO
336.5-1.5	RCW108	16 36 22	-48 46 18	0.20 [0.06]	-23		-25.0	1.6	12.9	6.5	H <sub>2</sub> CO
336.8+0.0		16 30 49	-47 30 24	[0.05]			-80.0	4.6	9.9	4.1	H <sub>2</sub> CO
336.9-0.1		16 32 09	-47 32 30	[0.06]			-73.0	4.2	10.3	4.3	H <sub>2</sub> CO
337.1-0.2		16 33 01	-47 25 18	[0.06]			-72.0	4.2	10.3	4.3	H <sub>2</sub> CO
338.0-0.1		16 34 14	-46 45 18	[0.05]			-52.0	3.2	11.4	5.0	H <sub>2</sub> CO
337.9-0.5*		16 37 27	-47 01 36	0.36 [0.03]	-40	4.2	-40.0	2.6	12.0	5.6	H <sub>2</sub> CO
338.1-0.1		16 36 14	-46 45 18	[0.06]			-40.0	2.6	12.0	5.6	H <sub>2</sub> CO
338.9+0.6		16 36 42	-45 34 24	0.30 [0.06]	-66	5.5	-63.0	3.9	10.8	4.5	H <sub>2</sub> CO
338.1-0.2		16 36 58	-46 41 54	[0.07]			-48.0	3.0	11.6	5.2	H <sub>2</sub> CO
338.4+0.0		16 37 10	-44 18 18	0.17 [0.01]	-38	54	-37.0	2.4	12.3	5.7	
338.9-0.1		16 39 36	-46 00 48	[0.04]			-40.0	2.6	12.1	5.5	
338.4-0.2		16 39 40	-46 29 36	[0.06]			-4.0	0.2	14.4	7.6	
340.3-0.2		16 45 19	-45 04 06	0.24 [0.04]	-45	3.5	-43.0	3.1	11.8	5.1	
340.8-1.0	RCW110	16 50 39	-45 12 12	0.36 [0.01]	-27	3.0	-25.0	1.8	13.1	6.2	H <sub>2</sub> CO, IRAS
345.0+1.5	RCW116	16 54 22	-40 19 36	[0.03]			-17.0	1.6	13.7	6.4	
345.3+1.5	RCW116	16 55 37	-40 09 24	0.10 [0.04]	-15.9		-15.0	1.4	13.9	6.5	
343.5+0.0		16 55 48	-42 30 12	[0.03]			-30.0	2.4	12.7	5.6	
345.4+1.4		16 56 10	-04 07 00	0.29 [0.04]	-16	3.4	-15.0	1.4	13.9	6.5	
351.4+0.7*	NGC6334	17 17 20	-35 45 48	1.50 [0.05]	-5	3.4	-4.0	0.6	14.9	7.3	H <sub>2</sub> CO
353.1+0.6	RCW131	17 22 18	-34 20 06	[0.06]			-5.0	1.0	14.7	6.9	
0.2+0.0		17 42 48	-28 45 53	0.46 [0.05]	50	31	-12.0				
0.5+0.0		17 43 56	-28 30 35	0.15 [0.05]	47	43	40.0				
0.7-0.1*	Sgr B2	17 44 14	-28 23 17	1.85 [0.07]	48	46	61.0				
6.1-0.1		17 56 52	-23 45 29	[0.03]			11.0	2.2	13.5	5.7	
6.6-0.1	RCW145	17 57 45	-23 18 59	[0.03]			15.0	2.7	13.0	5.2	
10.2-0.3	W31	18 06 23	-20 20 12	[0.02]			14.0	1.8	13.7	6.1	
15.0-0.7	RCW160	18 17 30	-16 13 06	[0.02]			19.0	1.7	13.5	6.3	

NOTE: The observed positions are H109 α peaks (Wilson 1970). Sources with asterisks attached to their names are known ammonia sources. The brackets attached to the observed intensity are the rms of the fitted baseline. At the positions where the (J,K)=(1,1) ammonia lines are close to the detection limit, with intensities smaller than 3 rms, the line widths are not given. In the last column IRAS means that there is an IRAS point source with color index of ultracompact HII region associated to the observed positions, and H<sub>2</sub>CO means that Whiteoak and Gardner (1974) detected formaldehyde toward this position.

their equatorial coordinates, Columns (5), (6) and (7) the NH<sub>3</sub> (J=K=1) antenna temperature, radial velocity, and line width respectively, Column (8) gives the H109 α radial velocity observed by Wilson et al. (1970), Columns (9), (10) and (11) their possible distances to the Sun and to the Galactic Center respectively, calculated from their radial velocities (when not forbidden) and the rotation curve given by Clemens (1985), assuming a distance from the Sun to the Galactic Center of 7.9 kpc (Reid 1989), and finally Column (12) contains some comments about the sources. Attached to the antenna temperatures are their errors, obtained from the rms of the base line fitting. The antenna temperatures were corrected for atmospheric attenuation but the line widths were not corrected for the spectral resolution of the acousto optical spectrometer.

Among the 108 HII regions observed in this survey, 30 presented ammonia emission. For another 11 positions, the antenna temperatures were smaller than 3 times the rms noise level and had NH<sub>3</sub> radial velocities displaced by less than 5 km s<sup>-1</sup> from the recombination line velocities. For these sources, the antenna temperatures are shown but no line widths are given.

## 4. Discussion

### 4.1. NH<sub>3</sub> in the direction of IRAS sources

Twelve of the 108 HII regions observed have associated IRAS sources with color indices of ultra compact HII regions. We con-

sider that an IRAS source is associated with the HII region when it is displaced by less than the telescope half power beam width from the observed position. These sources are listed in Table 2 where Columns (1) and (2) give the names of the ammonia and IRAS sources, (3) and (4) give the equatorial coordinates of the IRAS sources, (5) the distance in arc minutes between the observed positions and the IRAS sources, Column (6) through (9) give the IRAS fluxes, and finally Column (10) the luminosity obtained integrating the four uncorrected IRAS color bands. Attached to the flux density for each IRAS band is given the flux quality. It is remarkable that 7 of these positions have positive ammonia detection, while in the other 5 there is evidence of weak emissions. These results show that there is a high detection rate of NH<sub>3</sub> (≥ 0.6) when the observed position has an associated IRAS point source with color index of ultra-compact HII region. This detection rate is compatible with the rate of 70 % observed by Churchwell et al. (1990) toward northern hemisphere ultra-compact HII regions using the Effelsberg radio telescope.

### 4.2. Distribution of NH<sub>3</sub> sources in Galactic longitude

The distribution in Galactic longitude of the HII regions and the detected NH<sub>3</sub> sources are similar, as can be seen in Fig. 1. However, the distribution of HII regions presents two peaks, one between 330°–340° with 36 sources and the other between 280°–

**Table 2.** Compact IRAS Sources with Color Index of Ultra-Compact HII Regions

Gal. Coord (l+b)	IRAS name	RA (1950) (h m s)	Dec (1950) (° ' ")	$\Delta\Theta$ arcmin	Flux (Jy)			L $10^4 L_{\odot}$	
					12 $\mu$ m	25 $\mu$ m	60 $\mu$ m		
268.4-0.8	09002-4732(3)	09 00 12	-47 32 07	0.69	1201 [3]	1962 [3]	11880 [3]	14710 [3]	0.03
291.3-0.7	11097-6102(6)	11 09 45	-61 02 17	0.31	391 [3]	5957 [2]	10900 [3]	38550 [1]	21
301.0+1.2	12320-6122(5)	12 32 02	-61 22 52	0.16	80 [2]	351 [3]	5242 [3]	7970 [3]	-
305.2+0.2	13079-6218(1)	13 07 60	-62 18 47	3.00	28 [2]	250 [3]	3167 [2]	8164 [2]	4
311.6+0.3	14013-6105(4)	14 01 18	-61 05 45	0.31	13 [3]	162 [3]	2345 [3]	4567 [3]	5
316.8-0.1	14416-5937(1)	14 41 40	-59 37 21	1.17	140 [1]	766 [3]	6845 [3]	16100 [3]	5
326.7+0.6	15408-5356(3)	15 40 53	-53 56 31	0.81	163 [2]	1680 [3]	10500 [3]	16800 [3]	15
328.3+0.4	15502-5302(3)	15 50 17	-53 02 47	0.26	143 [3]	1210 [3]	11570 [3]	12620 [3]	64
332.8-0.6	16164-5046(3)	16 16 26	-50 46 10	1.15	105 [3]	1479 [3]	11380 [3]	20370 [3]	23
333.1-0.4	16172-5028(2)	16 17 13	-50 28 14	0.08	144 [2]	1514 [3]	12380 [3]	26700 [3]	20
333.3-0.4	16177-5018(2)	16 17 44	-50 18 00	1.31	181 [3]	2054 [3]	7964 [2]	25630 [3]	17
340.8-1.0	16506-4512(2)	16 50 39	-45 12 43	0.52	83 [3]	787 [3]	7541 [2]	11640 [3]	5

NOTE: The IRAS fluxes are not color corrected. In order to estimate the luminosity we integrated the flux density in frequency and used the source distance given in Table 1. Attached to the flux density in each frequency band, the IRAS flux quality is given

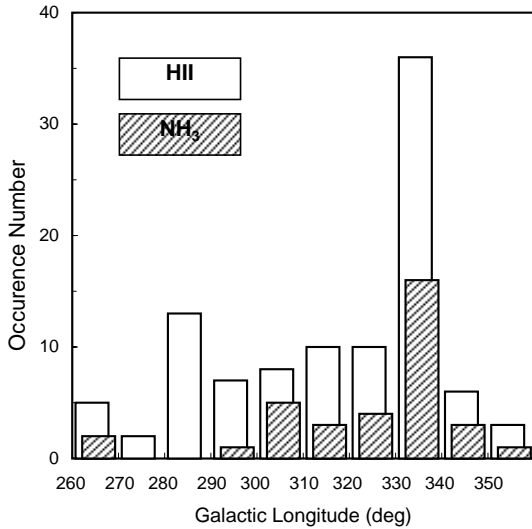


**Fig. 1.** Histograms, in galactic coordinates, of the distribution of selected HII regions and positions with positive NH<sub>3</sub> detection (hatched block).

290° with 13 sources. The NH<sub>3</sub> distribution also has a peak at 330°–340°, but does not present any source at the position of the second peak. Moreover, the region between 260°–290° has only two ammonia sources detected, compared with the 20 observed HII regions. Kinematic distances indicate that the two sources are in the solar neighborhood. To test the statistical significance of these results, we applied the Kolmogorov–Smirnov test to the samples. Using the complete distribution, we found an 88 % probability of both samples having the same distribution, while the probability increased to 99.9 % when only longitudes larger than 290° were considered. This result confirms the importance of the absence of NH<sub>3</sub> sources in the interval 260°–290°. This range of longitudes is located between the local Cygnus arm and the Perseus arm, at a distance from the Sun of more than 3 kpc. The absence of ammonia in this direction could be explained if the observed HII regions were located at larger distances from the Sun than others, but this is not the case. In fact, the sources G287.3-0.7 and 287.9-0.8, which are associated with the Carina Nebula, are located at about 2.7 kpc from the Sun and G291.3-

0.7 has a kinetic distance between 2.2 and 3.5 kpc. These are typical distances of sources seen in other directions.

The absence of NH<sub>3</sub> sources could also be explained if the HII regions were in a more advanced evolutionary state or if they were mass limited, with the molecular clouds surrounding them already dissociated. However, the existence of dense molecular gas observed in this longitude interval through formaldehyde absorption, and CO(1–0), HCO<sup>+</sup>(1–0) and CS(2–1) emission lines, seem to invalidate this argument (Whiteoak & Gardner 1974, Wouterloot & Brand 1989, Batchelor et al. 1981, Bronfman et al. 1996). Another possibility is that the physical conditions for the excitation of the ammonia molecule are no longer present, even if the molecule does exist. This argument can be discarded when we look at other molecules, like HCO<sup>+</sup> and CS which are excited under physical conditions similar to the metastable ammonia lines.

#### 4.3. Distribution of NH<sub>3</sub> sources with distance to the Galactic center (Fig. 3)

The parameter which differentiates the samples of HII and NH<sub>3</sub> sources at galactic longitudes between 280°–290° and 330°–340° is the distance to the Galactic Center. The region with no NH<sub>3</sub> emission, between 270° and 290°, is located far from the center, near or outside the solar orbit. Histograms of the distributions of the selected HII regions and detected ammonia sources as a function of distance to the Galactic Center are shown in Fig. 2. The graph of the observed HII regions shows an almost symmetric distribution with a peak at 6.5 kpc. The ammonia distribution has a peak at the same position but presents a strong asymmetry with a small number of ammonia sources at distances larger than 6.5 kpc. To obtain the statistical significance of this asymmetry we plotted the ratio of the number of ammonia sources to HII regions as a function of the distance to the Galactic center. A very well defined linear trend is found, with a slope of  $-0.08 \text{ kpc}^{-1}$  and a correlation coefficient  $r = 0.98$ . If, as discussed above, there is dense molecular gas associated with these HII regions and the physical conditions are favorable to NH<sub>3</sub> emission, then the decrease in the number of detected ammonia sources could be due to a decrease in their bright-

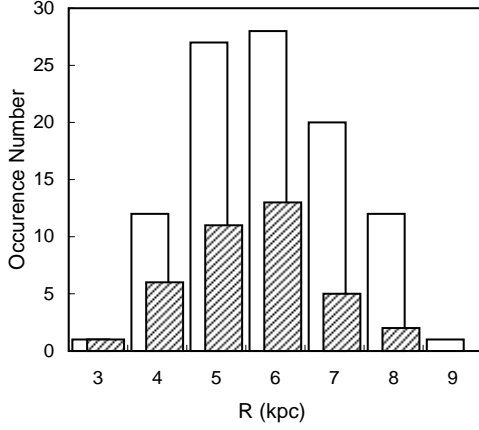


**Fig. 2.** Histograms, in distance to the galactic center of the observed HII regions and positions with positive ammonia detection (hatched block).

ness temperature, which puts them below the detectability limit of our radiotelescope. The decrease in brightness temperature could be due to a decrease in the ammonia abundance with the distance to the galactic center, as a consequence of the gradient in the nitrogen abundance. In fact, N and O abundance gradients of about  $-0.08 \text{ dex kpc}^{-1}$  have been identified in HII regions (Shaver et al. 1983; Simpson et al. 1995; Afflerbach et al. 1997), and in type II planetary nebulae (Maciel & Chiappini 1994).

#### 4.4. The distribution of NH<sub>3</sub> sources with brightness temperatures

The gradient of nitrogen abundance, the detection rates and the distribution of NH<sub>3</sub> sources with brightness temperature were used to determine the distribution of sources with H<sub>2</sub> column density. Several assumptions were made: (a) the brightness temperature of the source is proportional to the NH<sub>3</sub> abundance. This is valid for low optical depth, which is a good assumption since for more than 60 ammonia sources observed toward HII regions (MacDonald et al. 1981, Vilas-Boas et al. 1988, Churchwell et al. 1990) the average value of  $\tau(1, 1)$  is around unity, (b) the NH<sub>3</sub> abundance is proportional to the nitrogen abundance, true if the regions have similar H<sub>2</sub> and metal abundances (Graedel et al. 1982). The effects of other parameters, as cloud age, time to reach equilibrium, UV illumination, shocks and dust mantle destruction are supposed to be averaged, since we observe molecular clouds associated with HII regions in different stages of evolution. (c) the angular size of the molecular clouds where the ammonia sources are located is large compared with the radiotelescope beam, the consequences of this assumption will be discussed later, (d) the filling factor (fraction of the beam covered by the NH<sub>3</sub> sources) is the same for the whole cloud. This is true if the ammonia sources are formed by small high density clumps, uniformly distributed in the molecular cloud. Evidence in favor of this assumption are given by Stuzki & Winnewisser (1985), who showed that in order to explain the anomalies in the intensity of the hyperfine satellite inversion lines, it is necessary to assume that the NH<sub>3</sub> sources

are formed by a large number of independent clumps with sizes of the order of  $10^{-2}$  pc and masses of about a solar mass, (e) the kinetic temperature of each clump (or its distribution) is independent of the galactocentric distance. Although a gradient in kinetic temperature is observed in HII regions, where the main coolant is ionized oxygen, it is not expected in molecular clouds with temperatures smaller than 50 K, where the coolant is CO, which is optically thick in these dense regions. Assumptions (c) and (d) justify the subsequent use of measured antenna temperature  $T$  instead of brightness temperature.

Let us define  $f(T, R)$  as the fraction of the detected sources with temperature between  $T$  and  $T + dT$  at distance  $R$  from the Galactic Center. The total fraction of sources detected at distance  $R$  will be:

$$F(R) = \int_{T_{min}}^{T_{max}} f(T, R) dT \quad (1)$$

where  $T_{min}$  is given by the detection limit of the radiotelescope and  $T_{max}$  is the maximum temperature of the sources (the excitation temperature in the limit of an optically thick source). Since we assumed that the brightness temperature is proportional to the nitrogen abundance, we can write:

$$T(R) = T(R_0) \times 10^{-\alpha(R-R_0)} \quad (2)$$

where  $R_0$  is some reference distance at which the source temperature is  $T_0$  and  $\alpha = 0.07 \pm 0.01 \text{ dex kpc}^{-1}$  is the N gradient in the Galaxy (Maciel & Chiappini 1994).

Also, since we have assumed that the only difference between the molecular clouds at different distances is their NH<sub>3</sub> content, the sources at a distance  $R$  and temperatures between  $T$  and  $T + dT$  will have temperatures between  $T_0$  and  $T_0 + dT_0$  at the distance  $R_0$ . Therefore we can write:

$$f(T, R)dT = f(T_0, R_0)dT_0 \quad (3)$$

Eq. (1) becomes:

$$F(R) = \int_{T_{min}(R)}^{T_{max}} f(T_0, R_0)dT_0 \quad (4)$$

where now the minimum temperature is a function of  $R$ , given by:

$$T_{min}(R) = T_{min}(R_0) \times 10^{\alpha(R-R_0)} \quad (5)$$

The slope of  $F(R)$  will be:

$$\begin{aligned} \frac{dF}{dR} &= \frac{d}{dR} \int_{T_{min}(R)}^{T_{max}} f(T, R) dT \\ &= -f(T_{min}, R_0) \frac{dT_{min}(R)}{dR} \end{aligned} \quad (6)$$

From (4), (5) and (6) we obtain:

$$\frac{dF(R)}{dR} = -\alpha(\ln 10) T_{min}(R) f(T_{min}, R) \quad (7)$$

Comparing this expression with the best fit to our data in Fig. 3,  $F = -0.082R + 0.85$ , we conclude that  $f(T, R)$  should

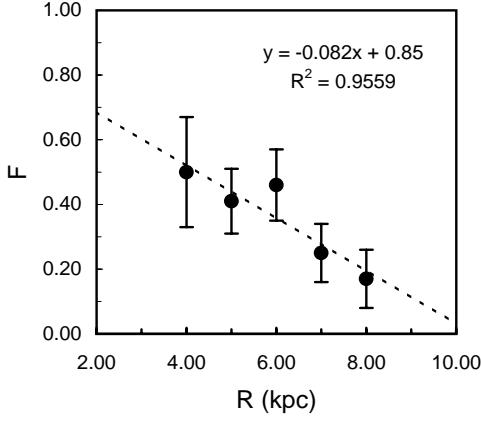


**Fig. 3.** Distribution of the fraction of detected ammonia sources ( $F$ ) as a function of the distance to the galactic center.

vary as  $T^{-a}$ , with  $a = 1$ . If the angular sizes of the molecular clouds are smaller than the radiotelescope beam size, the filling factors will decrease with distance to the observer. In this case, the real number of ammonia sources should be larger than the detected number at larger distances to the observer. The mean distance of the sources to the observer, on the other hand, increases as the galactocentric distance decreases, as can be seen in Fig. 4, for this reason we expect  $a \geq 1$ .

Under the assumptions listed at the beginning of this section, the brightness temperature reflects the NH<sub>3</sub> column density and, after corrections for the gradient in the abundance of this molecule with the galactocentric distance, it also represents the H<sub>2</sub> column density. Therefore, the distribution  $f(R, T) \propto T^{-1}$  indicates that the fraction of molecular clouds associated to HII regions decrease as the H<sub>2</sub> column density increases. Since the actual sizes of the molecular clouds are not known, we cannot convert H<sub>2</sub> column density to mass, but it is possible that the distribution of  $f(R, T)$  with  $T$  is a consequence of some relation  $f(M) \propto M^{-\beta}$ , where  $M$  is the mass of the cloud. Relations of this type are found in the distribution of clumps in  $\rho$  Oph (Motte et al. 1998) and also in other molecular clouds (Loren 1989, Blitz 1993), with  $\beta$  varying between 1 and 2.5.

Another quantity which can be calculated once the distribution of sources with  $T$  is known is the mean brightness temperature:

$$\begin{aligned} \langle T(R) \rangle &= \frac{\int_{T_{min}}^{T_{max}} T(R) f(T, R) dT}{\int_{T_{min}}^{T_{max}} f(T, R) dT} \\ &= \frac{T_{max} - T_{min}}{\ln(T_{max}/T_{min})} \end{aligned} \quad (8)$$

where we have assumed  $f(T, R) \propto T^{-1}$ . Using Eq. (2) we obtain:

$$\begin{aligned} \langle T(R) \rangle &\sim \frac{T_{max}}{\ln[T_{max}/T_{min}(R_0)]} \\ &\times \left[ 1 - \frac{\alpha \ln 10 (R - R_0)}{\ln[T_{max}/T_{min}(R_0)]} \right] \end{aligned} \quad (9)$$

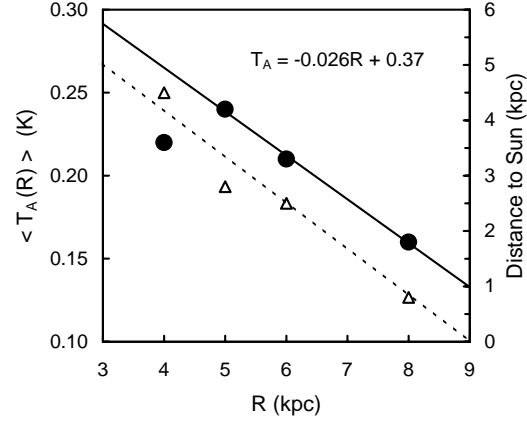


**Fig. 4.** Distribution of the mean temperature of the detected ammonia sources (dots) and mean distance to the observer (triangles) as a function of the distance to the galactic center.

and

$$\frac{d\langle T(R) \rangle}{dR} = \frac{\alpha T_{max} \ln 10}{\{\ln[T_{max}/T_{min}(R_0)]\}^2} \quad (10)$$

The maximum observed temperature is 1.5 K for NGC6334, the minimum temperature can be taken as 0.1 K, three times the rms of the observations, using these values and  $\alpha = 0.8$  in Eq. (9) we obtain  $d\langle T(R) \rangle / dR = 0.3\text{K/kpc}$

In Fig. 4 we present the calculated mean temperature for four interval bins in galactocentric distance. The three points at the largest distance to the Galactic Center define a line with slope 0.26, in agreement with the value derived in Eq. (9), however, the point closest to the Center falls well below this line. This behavior would be expected if the assumption that the sources cover completely the antenna beam is valid up to distances to the observer of about 3 kpc, as can also be seen from the figure. At this distance the antenna beam will correspond to a linear size of about 3.5 pc. Actual sizes of molecular clouds associated with HII regions, obtained by mapping, are available for only a few sources. For other ammonia sources, specially those observed towards compact HII regions, only one position was studied and the size of the region calculated from the filling factor, under the assumption of LTE. However, as mentioned before, Stutzki and Winnewisser (1985) showed that a large fraction of warm ammonia sources present anomalous intensities in the satellite lines, probably caused by the superposition of small dense clouds in non LTE. The filling factor, in this case, is interpreted as the ratio between the solid angle occupied by all the clumps and the solid angle of the antenna beam. This interpretation is different from the usual assumption that the size of the molecular cloud is the product of the antenna beam size and the filling factor. Therefore, molecular clouds can be larger than the beam size and still have filling factors smaller than one.

## 5. Summary and conclusion

In this paper we present NH<sub>3</sub>(1,1) line observations in 108 southern hemisphere HII regions. The main results of this re-

search are: (1) ammonia was detected in about 30 % of the observed positions, (2) no ammonia (1,1) line was identified above the three times the antenna temperature limit of 0.04 K in the 270°–290° galactic longitude interval, where 14 HII regions were observed, (3) ammonia was detected in about 60 % of the positions which had an associated IRAS point source with color index of ultra-compact HII regions, (4) it was found a gradient of about -0.08 in the fraction of NH<sub>3</sub> sources in the direction of HII regions, per kpc in galactocentric radius. and (5) the distribution of ammonia sources varies as  $T^{-1}$ , indicating, under certain assumptions, that the fraction of molecular clouds associated to HII regions decrease as the H<sub>2</sub> column density increases.

*Acknowledgements.* This work was partially supported by the Brazilian Agencies FAPESP and FINEP/PRONEX. The authors are grateful to the Eng.. Ricardo E. Schaal and Yaeer Bakor, and the staff members of the Itapetinga Observatory for the technical support during the observations and Dr. Jacques Lépine for helpful discussions. J. W. S. V. B. acknowledges Elizabete Aparecida do Amaral for helping with the observations.

## References

- Abraham Z., Kokubun F., 1992, A&A 257, 831  
 Afflerbach A., Churchwell E., Werner W.M., 1997, ApJ 478, 190  
 Batchelor R.A., McCulloch M.G., Whiteoak J.B., 1981, MNRAS 194, 911B  
 Blitz L., 1993, In: Levy E.H., Lunine J.I. (eds.) Protostars and Planets III, The University of Arizona Press, Tucson, p. 125  
 Bourke T.L., Hyland A.R., Robinson G., James S.D., Wright C.M., 1995a, MNRAS 276, 1067B  
 Bourke T.L., Hyland A.R., Robinson G., 1995b, MNRAS 276, 1052B  
 Bronfman L., Nyman L.-A., May J., 1996, A&AS 115, 81  
 Cheung A.C., Rank D.M., Townes C.H., Tharnton D., Welch W.J., 1968, Phys. Rev. Letters 21, 1701  
 Churchwell E., Walmsley C.M., Cesaroni R., 1990, A&AS 83, 119  
 Clemens D.P., 1985, ApJ 295, 422  
 Gardner F.F., Whiteoak J.R., Peters W.L., Kuipper T.B.H., 1985, Proc. ASA 6, 176  
 Graedel T.E., Longer W.D., Frerking M.A. 1982, ApJS 48, 321  
 Jauncey D.L., Batty M.J., Gray G.J., Moore R.C., 1981, Proc. Astron. Soc. Aust. 4, 262  
 Loren R.B., 1989, ApJ 338, 902  
 Maciel W.J., Chiappini C., 1994, Ap&SS 219, 231  
 McDonald G.H., Little L.T., Brown A.T., et al., 1981, MNRAS 195, 387  
 Motte F., André P., Neri R., 1998, A&A 336, 150  
 Myers P.C., Benson P.J., 1983, ApJ 266, 309  
 Scalise E.S., Schaal R.E., Bakor Y., Vilas-Boas J.W.S., Myers P.C., 1981, AJ 86, 1939  
 Shaver P.A., McGee R.X., Newton L.M., Dunks A.C., Pottasch S.R., 1983, MNRAS 204, 53  
 Simpson J.P., Sean, Colgan W.J., Rubin R.H., Erickson E.F., Haas M.R., 1995, ApJ 444, 721  
 Reid M.J., 1989, In: Morris R. (ed.) The Center of the Galaxy. Kluwer, Dordrecht, p. 37  
 Stutzki J., Winnewisser G., 1985, A&A 144, 13  
 Vilas-Boas J.W.S., Scalise E.J., Monteiro do Vale J.L., 1988 Ap&SS 141, 339  
 Wilson T.L., Mezger P.G., Gardner F.F., Milne D.K., 1970, A&A 6, 364  
 Wouterloot J., Brand J., 1989, A&AS 80, 149  
 Whiteoak J.B., Gardner F.F., 1974, A&A 37, 389